The Analysis of Harmonic Energy Distribution Portfolio for Digital-to-Frequency Converters

Liming Xiu, *Senior Member, IEEE,* Chen-Wei Huang, and Ping Gui, *Member, IEEE*

***Abstract*—Digital-to-Frequency Converters (DFC) based on the concept of Time-Average-Frequency and a Flying-Adder frequency synthesizer is a novel circuit component which enables many system-level innovations. The clock output of the DFC has unique characteristics both in time and frequency domains. In this paper, a study on the energy distribution of the DFC output for a special case is presented. Mathematical analysis is performed and closed-form expression is derived for this case.**

***Index Terms*— Digital-to-frequency Converter (DFC), Flying-Adder, PLL, Frequency Synthesis, Fourier Series.**

I. INTRODUCTION

A Digital-to-Frequency Converter (DFC) based on the concept of Time Average Frequency and Flying-Adder frequency synthesizer is a new circuit component introduced just recently [1-2]. Compared to Digital-to-Analog Converters (DACs) whose output is the *magnitude* of certain medium (voltage or current), the output of DFCs is frequency, or the *rate-of-switching* of the medium. The emerging DFCs can be used to represent information in the rate-of-switching style for information processing. This is similar to the role of DACs in the traditional magnitude-based information processing approach. This new approach using DFCs can potentially result in more cost-effective electronic systems design for certain applications.

Another important usage of DFCs is to function as the clock driver of VLSI systems. A majority of today's VLSI systems use synchronous design style controlled by clock signals. The proposed DFC has two important features: instantaneous frequency switching and the capability of generating arbitrary frequencies. These two features make the DFC a very attractive alternative as a clock driver.

The DFC is built on two cornerstones: a circuit implementation technique of Flying-Adder frequency synthesis architecture [3] and the concept of Time-Average-Frequency rigorously formed in [1]. The Flying-Adder architecture has been used in various commercial products for almost ten years, which has enabled many system-level innovations [4]. However, during the past practices of using this architecture in real applications, the Time-Average-Frequency concept is only used subconsciously and the theoretical understanding has not been established. Time-Average-Frequency, which is different from the conventional concept of frequency, has its unique characteristics both in time and frequency domains. These characteristics can significantly

L. Xiu is with Texas Instruments, Dallas, TX 75243 USA (email: lmngx96@gmail.com).
Chen-Wei Huang is with the Southern Methodist University, Dallas, TX 75205 USA (phone: 214-606-1869; e-mail: chenweih@smu.edu).
Ping Gui is with the Southern Methodist University, Dallas, TX 75205 USA (phone: 214-768-1733; e-mail: pgui@smu.edu).

impact the DFC's usage in real systems, especially when the DFC output is used as clock to drive systems with embedded analog blocks such as ADCs and DACs. In order to build a solid foundation for this new DFC component, reference [2] presents a formal request to the math and circuit communities for seeking help on seven DFC-related math problems. This paper is our attempt for understating issue #1 raised in [2].

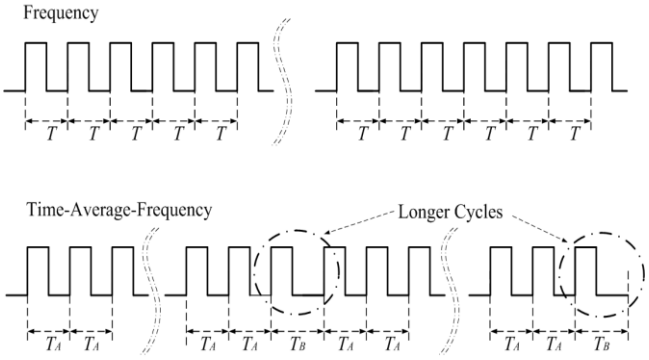

Fig. 1. The frequency and Time-Average-Frequency.

Figure 1 depicts the difference between the conventional frequency and Time-Average-Frequency. Unlike the case of conventional frequency where every clock cycles have the same length in time, the cycles in Time-Average-Frequency can have different lengths. However, within a certain timeframe (such as one second) the numbers of cycles are the same if both cases bear the same frequency (in Hz). The mathematical definition of both frequency and Time-Average-Frequency are established in [1].

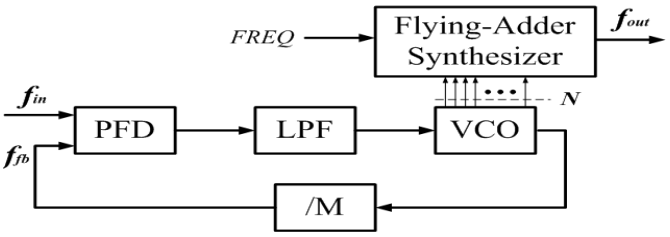

Fig. 2. The high-level block diagram of Flying-Adder PLL.

Figure 2 shows the high-level block diagram of the Flying-Adder Phase-Locked Loop based Frequency Synthesizer (FAPLL) that implements the Time-Average-Frequency concept in circuit. It is worth repeating that the FAPLL is the circuit hardware of the DFC, while the Time-Average-Frequency is the theoretical foundation.

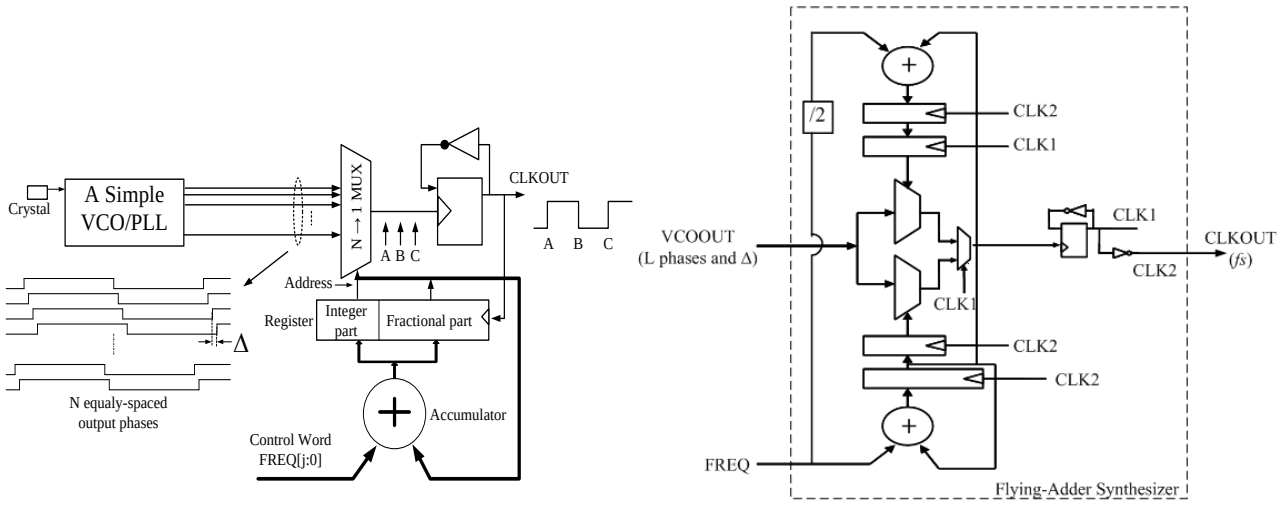

(a) (b)

Fig. 3. Flying-Adder frequency synthesizer: a) the principal idea. b) the working circuit.

As shown in Figure 3a), the FAPLL produces desired frequency from a group of equally-spaced VCO outputs. This multi-stage VCO provides multiple reference signals with the same frequency but evenly distributed phases to the frequency synthesizer. An accumulator with a frequency control word FREQ as the input produces the right select signals to a multiplexer which selects certain VCO output at certain time. The output of the multiplex triggers a DFF to generate the final clock output. Figure 3b) shows the working circuit of the Flying-Adder synthesizer which is used in real applications. The detailed explanation can be found in [3]. Unlike the conventional PLL-based frequency synthesis techniques, this architecture synthesizes frequencies outside the PLL loop, therefore resulting in an instant switching to any new desired frequencies.

Assuming the period of the *N*-stage VCO is T_{VCO}, the time difference between any two adjacent VCO outputs is given by:

$$\Delta = T_{VCO}/N \qquad (1)$$

To synthesize an output clock with frequency of $F = 1/T$, $FREQ$ is set by the following equation [3]:

$$T = \frac{1}{F} = FREQ \cdot \Delta$$

Or,

$$FREQ = \frac{1}{F \cdot \Delta} = \frac{N}{F \cdot T_{VCO}} \qquad (2)$$

$FREQ$ is a real number which can have integer part I and fractional part r, denoted as

$$FREQ = I + r. \qquad (3)$$

If $r = 0$, the FA synthesizer works in the integer mode; otherwise in the fractional mode. In the integer mode the synthesized

clock waveform has a uniform length in time for every cycle. In the fractional mode, the FA synthesizer employs two different cycles, T_1 and $T_1+\Delta$ to achieve the desired average frequency $F=1/T$, where T is the average clock period, and $T_1 < T < T_1+\Delta$. The frequency of the ($T_1+\Delta$) occurrence is determined by the value of r. By utilizing the two different types of cycles T_1 and $T_1+\Delta$ (corresponding to T_A and T_B in Figure 2), high frequency resolution can be achieved. By definition, the short cycle T_1 is given by

$$T_1 = I \cdot \Delta = I \cdot T_{VCO}/N \qquad (4)$$

For a clock signal with a uniform period T, the energy is concentrated at its fundamental frequency $1/T$ and its harmonics. For the Time-Average-Frequency clock, the uneven clock lengths caused by Δ introduce frequency modulation on the clock and change the energy distribution portfolio. It is of great interest, from the system point of view, to understand the frequency domain characteristics of this clock so that we can manipulate its frequency spectrum to our advantage.

A similar problem has been studied in Direct Digital Frequency Synthesizer (DDS) related research [5-8]. Structurally, the issue in DDS is rooted from the same circuit operation as in our DFC case: the loss of certain information when some digital bits are truncated. In DDS, this results in non-uniform sampling points, which will produce spurious components in the DDS's final output. In the Flying-Adder based DFC, this truncation results in uneven cycles. Another difference is that in DDS sinusoidal waveform is the point of interest whereas in DFC, the clock output is square waveform (pulse train). The spectrum of the Pulse Rate Frequency Synthesizer was studied in [9]. In this technique, the new frequency tone is generated by adding or subtracting pulses periodically which is different from the cycle-length adjustment used in Flying-Adder DFC technique. A recent work [10] has studied a similar problem as in this paper, but that work primarily relies on numerical solution. In this paper, the aim is to analytically study the Flying-Adder-based DFC's spectra energy distribution.

The paper is organized as follows. Section II develops a waveform decomposition technique, for a special case, to transfer the Time-Average-Frequency waveform to a group of pulse trains. Fourier analysis is then carried out on these pulse trains. Section III studies the average frequency and the maximum energy location, and proves that maximum energy occurs at the average frequency for this special case. Section IV presents the simulation results to the theoretical analysis. Section V concludes the paper.

II. WAVEFORM DECOMPOSITION AND FOURIER ANALYSIS

To understand the frequency domain characteristics and the energy distribution portfolio of the Time-Average-Frequency clock, Fourier analysis could be applied to the minimum portion of the waveform that repeats itself. This approach is straightforward in processing, but the closed-form expression cannot be obtained as demonstrated in [1]. In this paper, we attack this problem from a new angle: decomposing the Time-Average-Frequency clock into a group of pulse trains.

A. A simple case for demonstrating the technique

The time domain characteristic of a general Time-Average-Frequency clock waveform is shown earlier in Figure 1 (the bottom plot). Although seemingly simple, the task of obtaining the frequency domain characteristic is not trivial since the longer cycle T_B can occur in any pattern. For this reason, we start with a simple yet instructive case where the fractional portion of *FREQ* takes the value of $r = 0.5$. Figure 4 shows the waveforms of *FACLK* (a Time-Average-Frequency clock) and *ICLK*. *ICLK* is an ideal clock with frequency of $F = 1/T$ which is used as a reference for comparison.

Both *FACLK* and *ICLK* bear the same frequency when measured in certain time frame, such as one second. For *FACLK*, the case of r = 0.5 corresponds to the scenario where cycle $T_A = T_1$ and cycle $T_B = T_1 + \Delta$ occurring alternately with the same rate, as shown in Figure 4. It is clear that *FACLK* has the period of $2T$ (repeating itself every $2T$) but an average frequency of $F = 1/T$.

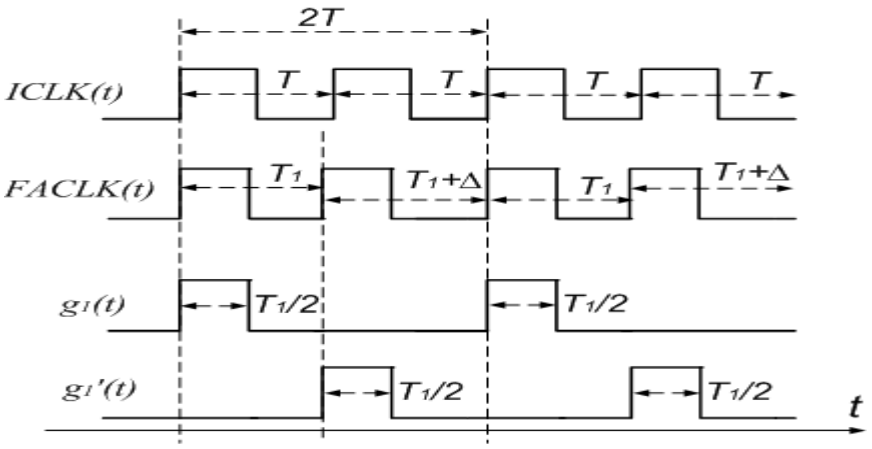

Fig. 4. The ideal clock *ICLK*, Flying-Adder clock *FACLK* of r = 0.5, $g_1(t)$, and $g_1'(t)$.

To facilitate the mathematical analysis, *FACLK* is decomposed into two periodic pulse trains, $g_1(t)$, and its time shifted version, $g_1'(t)$, as shown in Fig. 4[1]. Since all signals are periodic, Fourier series is used to obtain the frequency spectrum.

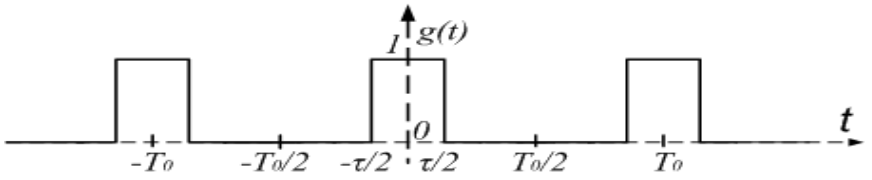

Fig. 5. A periodic pulse train signal.

For a generic pulse train signal shown in figure 5, the Fourier coefficients can be calculated by

$$c_k = \frac{1}{T_0}\int_{-T_0/2}^{T_0/2} g(t)\cdot e^{-j2\pi k\ F_0 t}\cdot dt$$
$$= \frac{1}{T_0}\int_{-\frac{\tau}{2}}^{\frac{\tau}{2}} e^{-j2\pi k\ F_0 t}\cdot dt\ = \frac{\sin(\pi k\ F_0\tau)}{\pi k} \qquad (5)$$

where $k = \pm 1, \pm 2, \ldots$, T_0 is the period of the pulse signal, τ is the width of the pulse, and $F_0 = 1/T_0$ is the fundamental frequency of this periodical signal. For *ICLK* with uniform period T and frequency F, we have $F_0 = 1/T = F$. For *FACLK* of the same average frequency F but with r = 0.5, its period is $2T$. Consequently, its fundamental frequency $F_0 = 1/(2T) = F/2$, which is half that of *ICLK*.

The Fourier series coefficients of *ICLK* can be obtained by plugging $\tau = \frac{T}{2}$, and $T_0 = \frac{1}{F0} = T$ into (5). By doing so we have

[1] In the FA architecture, the prolonged portion with Δ only happens when clock voltage level is low. The duration of the clock being high in one period is always $T_1/2$.

$$c_k = \frac{\sin(\frac{1}{2}\pi k)}{\pi k} \qquad (6)$$

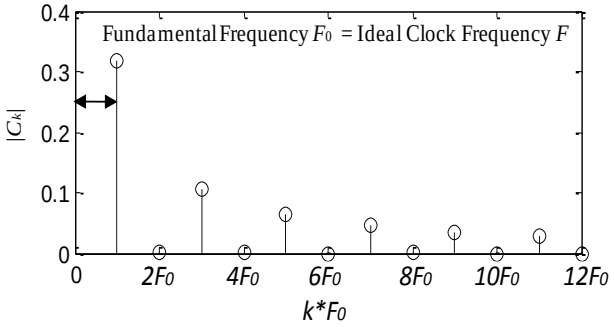

Fig. 6. Fourier coefficients (absolute value) of the *ICLK*.

Figure 6 plots the $|c_k|$ of *ICLK* (the DC component is omitted since it is irrelevant to this study). As expected, the maximum energy (the strongest harmonic stem) locates at the 1st harmonic with $k = 1$, and the maximum value is calculated using (6) as

$$c_1 = \frac{1}{\pi} \approx 0.3183 \qquad (7)$$

The first harmonic is at the frequency of *ICLK*, denoted as *F* previously.

After decomposition, *FACLK* becomes the combination of $g_1(t)$ and $g_1'(t)$. Likewise, the Fourier coefficients of $g_1(t)$ and $g_1'(t)$ can be derived by using (5) as well. Note that $g_1(t)$ and $g_1'(t)$ both have a period of $T_0 = 2T$ (as shown in Figure 4). In addition, $g_1(t)$ and $g_1'(t)$ are identical except for a time shift of T_1.

Plugging $\tau = \frac{T_1}{2}$ and $T_0 = 2T$ in (5), we obtain the Fourier coefficients of $g_1(t)$ as

$$c_k = \frac{\sin(\pi k \frac{T_1}{4T})}{\pi k} \qquad (8)$$

and the Fourier coefficients of $g_1'(t) = g_1(t - T_1)$ as

$$c_k = \frac{\sin(\pi k \frac{T_1}{4T})}{\pi k} \cdot e^{-\frac{j\pi k T_1}{T}} \qquad (9)$$

Combining (8) and (9) yields the Fourier coefficients of the *FACLK* as

$$c_k = \frac{\sin(\pi k \frac{T_1}{4T})}{\pi k} \cdot (1 + e^{-\frac{j\pi k T_1}{T}}) \qquad (10)$$

In (10), T is the period of *ICLK* and T_1 is the shorter cycle in *FACLK*. From Figure 4, we know $2T_1 + \Delta = 2T$, or $T_1/T = 1 - \Delta/(2T) = I/(I+0.5)$ which is a fixed number when *FREQ* is given. Figure 7 shows the Fourier coefficients of the *FACLK*, where *r*

= 0.5 and *I* takes the values of 2, 8 and 14, respectively.

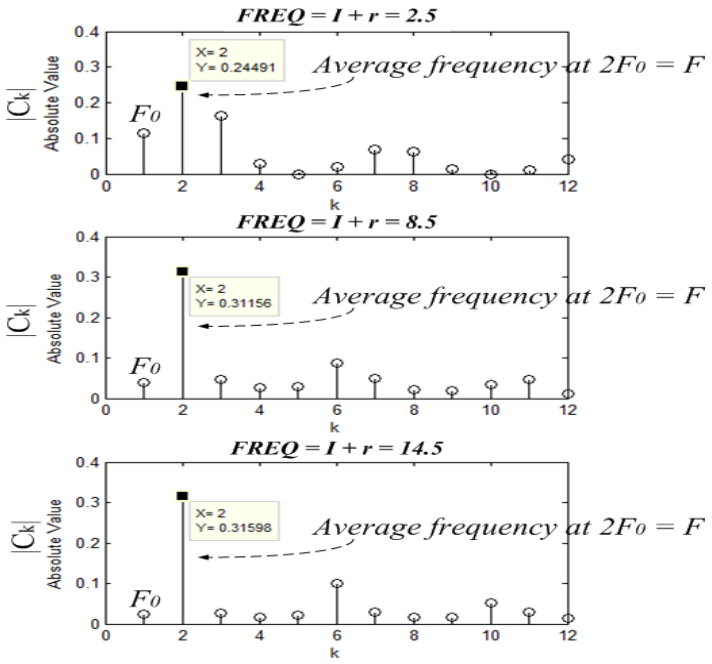

Fig. 7. Fourier coefficients of *FACLK* with r = 0.5.

It is interesting to see that, for all the three cases of r = 0.5, the strongest harmonic stems are all located at the 2nd harmonic, which is exactly the location of the average frequency $F = 2F_0$. Also worth mentioning is that, as *I* increases, a) the magnitude of the 2nd harmonic approaches its theoretical limit of 0.3183, b) the magnitude of F_0 becomes smaller, and c) the energy distribution portfolio resembles more of that of *ICLK*. The statement of c) is evident in Figure 7. The 2nd, 6th and 10th harmonics correspond to 1st, 3rd and 5th harmonics in Figure 6. This is due to the fact that the degree of dissimilarity between the waveforms of *ICALK* and *FACLK* diminishes when *I* increases.

B. A more general case of *r=1/R*

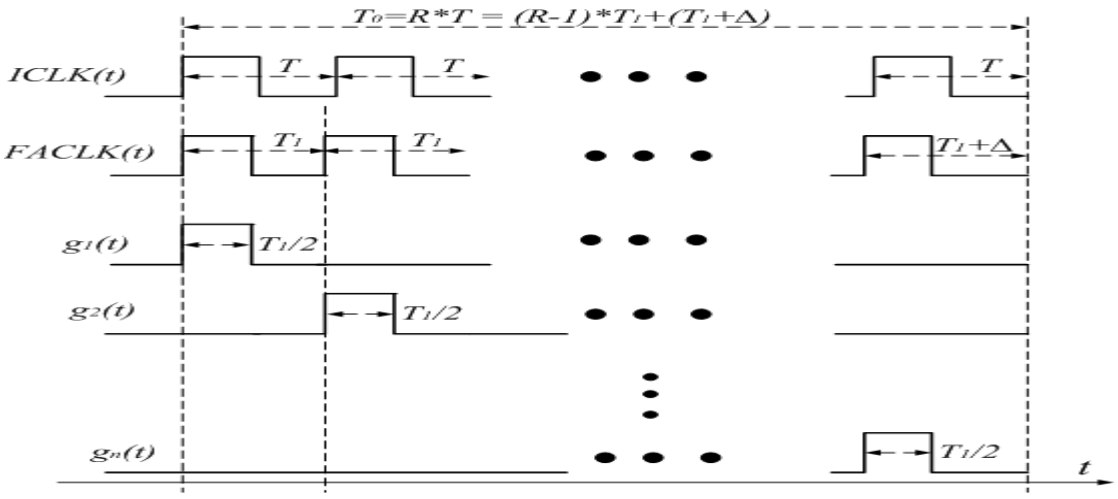

Fig. 8. The waveforms of the ideal clock *ICLK* and Flying-Adder clock *FACLK* of r = 1/*R*.

The approach in the previous section can be extended to a more general case of $r = 1/R$, where R is any integer equal to or greater than 2. Under this assumption, the synthesized clock has a cycle pattern of $T_1T_1T_1\ldots(T_1+\Delta)$, which consists of ($R$-1) cycles of T_1 followed by one cycle of ($T_1+\Delta$) as shown in Figure 8. In this case, the pattern repeats itself for every T_0 cycles where $T_0 = R \cdot T$ and the fundamental frequency becomes

$$F_0 = \frac{1}{T_0} = \frac{1}{RT} = \frac{1}{R}F \qquad (11)$$

As shown in Figure 8, the waveform of *FACLK* for $r=1/R$ can be decomposed into $g_1(t)$, and its time shifted versions $g_2(t)$, … $g_n(t)$ with a time shift of T_1 between any adjacent two. The *FACLK* waveform is the summation of these pulse trains, i.e. $y(t) = \sum_{n=1}^{R} g_n(t)$. Consequently, the Fourier coefficients can be calculated as:

$$c_k = \frac{\sin(\pi k \frac{T_1}{2RT})}{\pi k} \cdot \sum_{n=1}^{R} e^{-j2\pi \frac{kT_1}{RT}\cdot(n-1)} \qquad (12)$$

Equation (12) will be used for studying the frequency domain characteristics in the following section. The relationship between T_1 and T can be deducted as follows. From Figure 8, we know $R\cdot T_1 + \Delta = R\cdot T$, and from (2), $T = FREQ\cdot\Delta = (I + r)\cdot\Delta$, therefore we have the following relationship between T_1 and T.

$$\frac{T_1}{T} = \frac{1}{1+r/I} \qquad (13)$$

III. The Average Frequency and Maximum Energy

Section II develops a waveform decomposition method which transfers the Time-Average-Frequency clock into a group of pulse trains for the special case where the fractional part $r = 1/R$. Closed-form Fourier analysis of the Time-Average-Frequency clock is obtained as the sum of the Fourier series of the pulse trains, shown in (12). In this section, using (12), we will investigate the energy distribution among the harmonics and the energy associated with the average frequency.

A. Finding $|c_k|$'s maximum analytically

The energy distribution among the harmonics can be computed based on (12). In order to find the magnitude of c_k, we reorganize c_k in (12) as

$$c_k = \frac{\sin\left(\pi k \frac{T_1}{2RT}\right)}{\pi k} \cdot \sum_{n=1}^{R}\{\cos(2\pi \frac{k}{R}\frac{T_1}{T}\cdot(n-1)) - jsin(2\pi \frac{k}{R}\frac{T_1}{T}\cdot(n-1))\}$$

$Let\ c_k = a_k - jb_k$, where

$$a_k = \frac{\sin(\pi k \frac{T_1}{2RT})}{\pi k} \cdot \sum_{n=1}^{R} \cos(2\pi \frac{k}{R}\frac{T_1}{T} \cdot (n-1))$$

$$b_k = \frac{\sin(\pi k \frac{T_1}{2RT})}{\pi k} \cdot \sum_{n=1}^{R} \sin(2\pi \frac{k}{R}\frac{T_1}{T} \cdot (n-1))$$

From [11], we know the following:

$$\sum_{m=0}^{M} \sin(\varphi + m\alpha) = \sin(\frac{(M+1)\alpha}{2}) \cdot \sin(\varphi + \frac{M\alpha}{2}) / \sin(\frac{\alpha}{2})$$

$$\sum_{m=0}^{M} \cos(\varphi + m\alpha) = \sin(\frac{(M+1)\alpha}{2}) \cdot \cos(\varphi + \frac{M\alpha}{2}) / \sin(\frac{\alpha}{2})$$

Let $\varphi = 0, M = R-1, \alpha = 2\pi \frac{k}{R}\frac{T_1}{T}$, a_k and b_k become

$$a_k = \frac{\sin(\frac{\alpha}{4})}{\pi k} \cdot \frac{\sin(\frac{R\alpha}{2}) \cdot \cos(\frac{(R-1)\alpha}{2})}{\sin(\frac{\alpha}{2})}$$

$$b_k = \frac{\sin(\frac{\alpha}{4})}{\pi k} \cdot \frac{\sin(\frac{R\alpha}{2}) \cdot \sin(\frac{(R-1)\alpha}{2})}{\sin(\frac{\alpha}{2})}$$

Since $|c_k| = \sqrt{{a_k}^2 + {b_k}^2}$, substituting a_k and b_k into c_k yields

$$\sqrt{{a_k}^2 + {b_k}^2} = \left| \frac{\sin\left(\frac{\alpha}{4}\right)}{\pi k} \cdot \frac{\sin\left(\frac{R\alpha}{2}\right)}{\sin\left(\frac{\alpha}{2}\right)} \right| = \left| \frac{\sin(\frac{\alpha}{4})}{\pi k} \cdot \frac{\sin\left(\frac{R\alpha}{2}\right)}{2 \cdot \sin\left(\frac{\alpha}{4}\right) \cdot \cos\left(\frac{\alpha}{4}\right)} \right|$$

Replacing $\alpha = 2\pi \frac{k}{R}\frac{T_1}{T}$, we have

$$|c_k| = \left| \frac{1}{2\pi} \cdot \frac{1}{k} \cdot \frac{\sin\left(\pi k \frac{T_1}{T}\right)}{\cos\left(\pi \frac{k}{2R}\frac{T_1}{T}\right)} \right| = \left| \frac{T_1}{4RT} \cdot \frac{1}{\gamma} \cdot \frac{\sin(2R\gamma)}{\cos(\gamma)} \right| \qquad (14)$$

where $\gamma = \alpha/4 = \pi \frac{k}{2R}\frac{T_1}{T}$. When *FREQ* (=*I*+*r*) is given, T_1/T is fixed (refer to (13)), thus $|c_k|$ only depends on *k*.

To the first order, the maximum value of $|c_k|$ only occurs with the smallest *k* that makes cos(γ) = 0 (refer to the appendix for proof). Therefore, by setting $\gamma = \pi \frac{k}{2R}\frac{T_1}{T} = \frac{\pi}{2}$ in (14), the value of *k* that makes $|c_k|$ maximum can be found as:

$$k = R\frac{T}{T_1} = R + 1/I \qquad (15)$$

By using *L'Hopital's Rule* [11], the maximum of $|c_k|$ can be deducted as (see appendix):

$$|c_k|_{max} = \frac{1}{\pi} \cdot \frac{1}{1 + r/I} \qquad (16)$$

It is interesting to see that $|c_k|_{max}$ becomes $c_1 = \frac{1}{\pi}$ if r = 0, the same as in (7). This is due to the fact that *FACLK* and *ICLK* are identical when r = 0. Equation (16) approaches $\frac{1}{\pi}$ as I increases, which can also be understood intuitively.

Using (14), we can numerically plot $|c_k|$ as a function of k, where k is treated as a real variable. Figure 9 shows the plots that confirm that $|c_k|$ assumes the maximum value when k is the smallest number that makes $cos(\pi \frac{k}{2R} \frac{T_1}{T}) = 0$ (to the first order). They are around 4.125, 5.125 and 8.125 respectively.

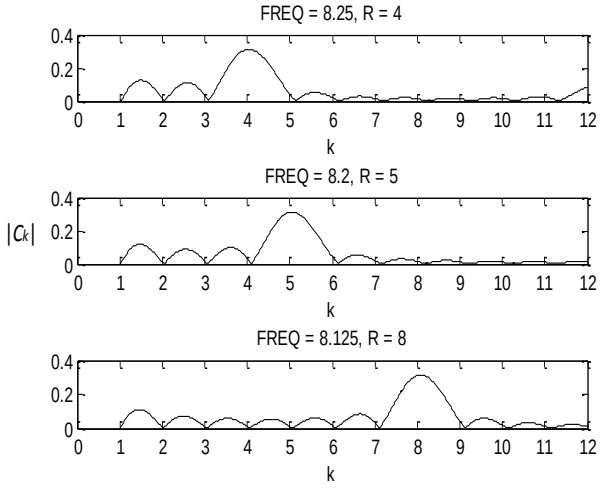

Fig. 9. Plots of $|c_k|$ with different *R (=1/r).*

B. The integer k which makes $|c_k|$ maximum

Section III.A shows that $|c_k|$ takes its maximum at $k = R + 1/I$ when k is treated as a real variable. However, in reality k can only be an integer since only the harmonics of the fundamental frequency F_0 is observable in Fourier analysis. The two nearby integers are $k = R$ and $k = R$+1. One of them is the harmonic which bears the maximum$|c_k|$, the strongest harmonic stem.

As discussed previously, k being $R + 1/I$ will make $\gamma = \pi/2$ and $2R\gamma = R\pi$. Around these values, both the *cos* and *sin* functions are symmetric. Therefore, function $\left|\frac{\sin(2R\gamma)}{\cos(\gamma)}\right|$ is symmetric around $k = R + 1/I$ as well. Between the two values of R and R + 1, $k = R + 1/I$ is closer to R for all the values of I greater than 2. Additionally, the term of $\frac{1}{2\pi} \cdot \frac{1}{k}$ in $|c_k|$ decreases monotonically with k. Own to the above facts, it is clear that $k = R$ is the integer value that makes the $|c_k|$ maximum.

Referring back to Figure 8 and equation (11), the fundamental frequency is $F_0 = F/R$. Therefore, the R^{th} harmonic location is exactly where the average frequency F is. In other words, for a Time-Average-Frequency waveform generated by the Flying-Adder PLL, when the control word takes the form of *FREQ = I + 1/R*, the strongest stem in its frequency spectrum is the R^{th} harmonic. This is also the location of the average frequency. The unit is the fundament frequency, which is the minimum portion in the clock waveform that repeats itself.

C. The impact of I on the clock energy distribution

The integer portion of *FREQ*, *I*, has a significant impact on the energy distribution of the Time-Average-Frequency clock. As demonstrated above, *FACLK* has the maximum energy at the average frequency F ($k = R^{th}$ harmonic) whereas the theoretical

maximum energy $\frac{1}{\pi}\cdot\frac{1}{1+r/I}$ happens at $k = R\frac{T}{T_1} = R + 1/I$. The distance between the two k values is $1/I$, which is inversely proportional to I. Figure 10 graphically illustrates this point for I = 3, 5, and 8, respectively. The calculated value from (15) is 4.333, 4.2 and 4.125 for each of the three cases, respectively. Figure 10 shows the results obtained from numerical approach, which are close but not exactly equal to the calculated ones. The reason of the small difference is due to the first-order approximation used when deriving (15). However, the statement that the harmonic with maximum energy is the R^{th} harmonic is true for all the cases (the 4th harmonic in these cases). It is this statement that is important in guiding the DFC usage in real applications.

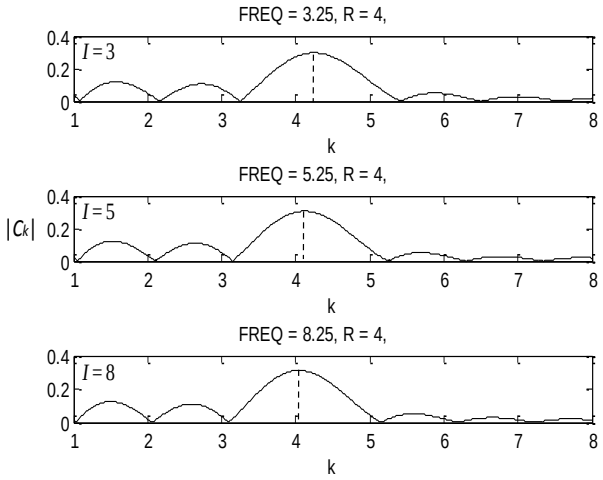

Fig. 10. Plots of $|c_k|$ with different I.

Moreover, Figure 11 shows that the magnitude of the $|c_k|_{k=R}$ gradually approaches its theoretical maximum of $|c_k|_{max} = \frac{1}{\pi}\cdot\frac{1}{1+r/I}$ as I increases. This can be understood intuitively since T_1 and T (referring to Figure 8) becomes more similar when I increases.

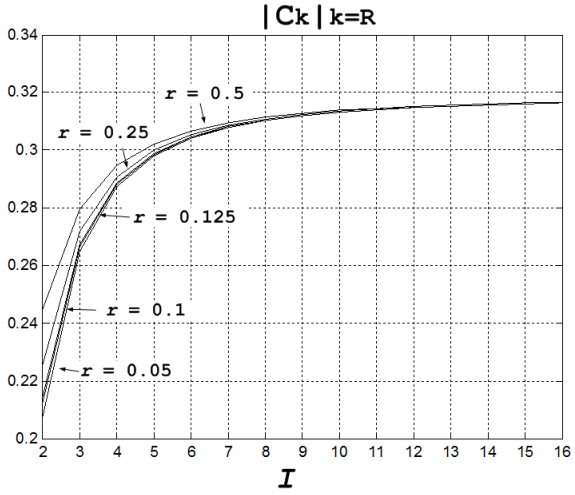

Fig. 11. Plots of $|c_k|_{k=R}$ vs I.

D. The impact of R on the clock energy distribution

Using (14), we can also plot $|c_k|_{k=R}$ as a function of *R* as shown in Figure 12. This plot depicts an important point: for a reasonably large *I* (>4), the percentage of energy allocated to the average frequency (R^{th} harmonic) is almost independent of *R*. The difference is only observable at the distribution of the rest of the energy among the other harmonics. For smaller *R* (meaning the T_B cycle in Figure 2 occurs more often), the spurious energy is distributed among several discrete locations with a few significant harmonics in telephone-pole-like form. For larger *R*, the spurious energy is more evenly distributed into many smaller magnitude spurious components with many insignificant harmonics in comb-like format. This statement will be demonstrated by the circuit simulation in the next section. Furthermore, Figure 11 and Figure 12 reveal another important fact: the larger the *I* is, the more the energy is allocated to the average frequency. This is another useful guideline for the DFC usage in real applications.

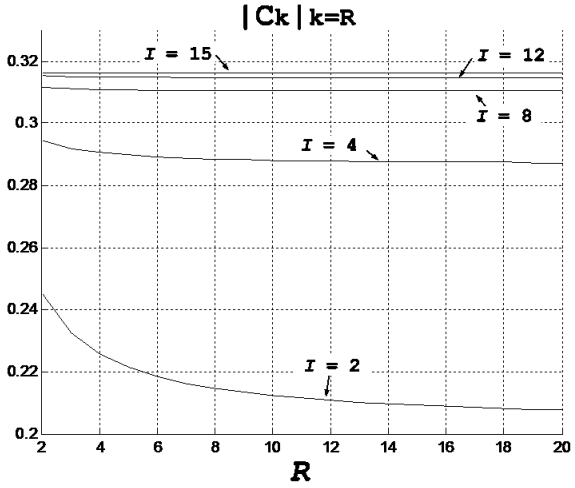

Fig. 12. Plots of $|c_k|_{k=R}$ vs *R*.

IV. SIMULATION

Section II develops a unique waveform decomposition technique, which is used to transfer the Time-Average-Frequency waveform into pulse trains for a special case. The closed-form expression of Fourier analysis is only obtained after this waveform transformation. Using this result, section III formally proves that, for Time-Average-Frequency in the form of *FREQ = I + 1/R*, the maximum energy locates at the R^{th} harmonic which is also the defined average frequency. In this section, we will present circuit-level simulations.

Using the CppSim simulator [12], a model of the Flying-Adder PLL in Figure 3 is created. The input reference frequency, f_{in}, is 20 MHz and the divider *M* = 50. Therefore, the VCO is running at f_{vco} = 1 GHz ($T_{VCO} = 1\,ns$). The VCO consists of 4 differential stages, thus it has eight outputs, i.e., *N* = 8.

Figure 13 shows the simulation when *FREQ* = 8.01 (*R* = 1/*r* = 100). From (2), we know that the output average frequency $F = \frac{N}{FREQ \cdot T_{VCO}} = \frac{8}{8.01 \cdot 1\ ns} = 0.99875$ GHz. The fundamental frequency $F_0 = F/R$ = 9.99 MHz. Figure 14 shows the case where *FREQ* = 8.333 and $F = \frac{N}{FREQ \cdot T_{VCO}} = \frac{8}{8.333 \cdot 1\ ns} = 0.96$ GHz. In this case, the fundamental frequency $F_0 = F/R$ = 320 MHz. It is clear that, in the case of *FREQ* = 8.01, the spurious energy is more evenly distributed among many harmonics with weak magnitudes, spaced by 9.99 MHz (comb-like). While in the *FREQ* = 8.33 case, the spurious energy is distributed among several strong harmonics which are spaced by 320 MHz (telephone-pole-like). In both cases, the energies allocated to the average

frequencies (the main stems) are almost the same as predicated by Figure 12. In these plots the energy between the spurious tones is due to the FFT leakage with no window function applied.

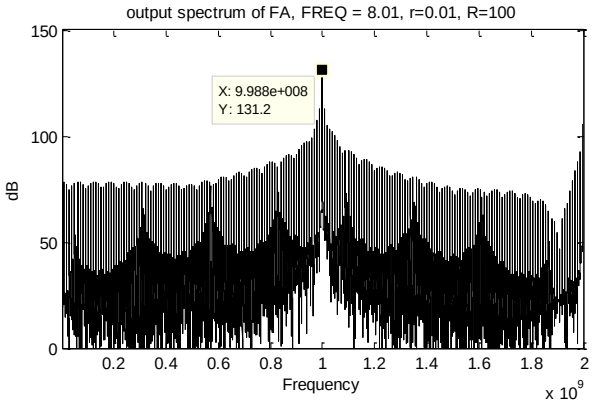

Fig. 13. CppSim behavior level simulation of FREQ = 8.01.

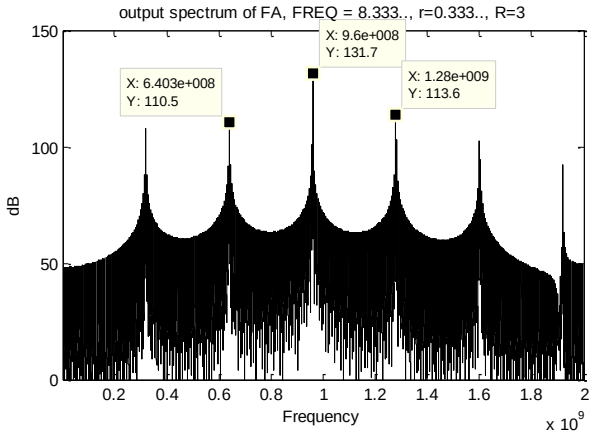

Fig. 14. CppSim behavior level simulation of FREQ = 8.333.

The circuit level simulation in SPICE is also performed on the circuits designed in IBM 0.13um CMOS technology. Figure 15 shows the SPICE simulation with *FREQ* = 8.25 (*R* = 4). As a comparison, Figure 16 is the CppSim simulation of *FREQ* = 8.25. The output average frequency $F = \frac{N}{FREQ \cdot T_{VCO}} = \frac{8}{8.25 \cdot 1\ ns} = 0.9697$ GHz, and the fundamental frequency $F_0 = F/R$ = 242 MHz. As can been seen, Figure 15 matches Figure 16 well in terms of the locations of the average frequency and the spectral spurs. The average frequency shown in both simulations agrees with the calculated value obtained from (2). The frequency component with maximum energy appears at the 4th harmonic as expected.

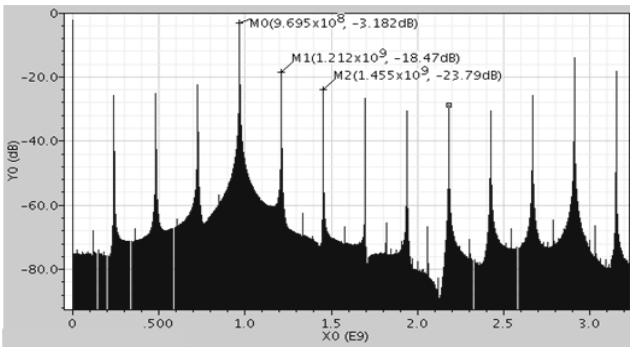

Fig. 15. Circuit level SPICE simulation of FREQ = 8.25.

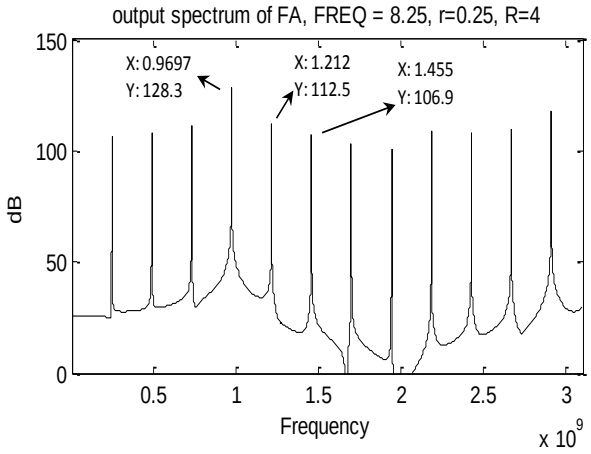

Fig. 16. CPP simulation of FREQ = 8.25.

V. CONCLUSION

In this paper, a unique waveform decomposition technique is developed. When applied to the special case of Time-Average-Frequency clock with $r = 1/R$, the closed-form Fourier coefficients are obtained. Using this result it is formally proved that the maximum energy accompanies the defined average frequency. Theoretically, this is an important result in that it has advanced our knowledge on this emerging Digital-to-Frequency Converter. This work makes us one step closer to the full understanding of the complex and important issues regarding the energy distribution portfolio of the DFC output. It can function as a step stone for further understanding of more complex issues, such as the general case of r = a/b where a and b are whole numbers.

VI. APPENDIX

In (14) of section III.A, it is derived that:

$$|c_k| = \left|\frac{T_1}{4RT} \cdot \frac{1}{\gamma} \cdot \frac{\sin(2R\gamma)}{\cos(\gamma)}\right| \qquad \text{(A-1)}$$

In this appendix, we will find the maximum value of $|c_k|$ and search the γ that results in the maximum of $|c_k|$.

$$\frac{d}{d\gamma}\left(\frac{1}{\gamma}\cdot\frac{\sin(2R\gamma)}{\cos(\gamma)}\right)=\frac{1}{\gamma}\cdot\frac{d}{d\gamma}\left(\frac{\sin(2R\gamma)}{\cos(\gamma)}\right)+\frac{\sin(2R\gamma)}{\cos(\gamma)}\cdot\frac{d}{d\gamma}\left(\frac{1}{\gamma}\right)=\frac{1}{\gamma}\cdot\frac{d}{d\gamma}\left(\frac{\sin(2R\gamma)}{\cos(\gamma)}\right)+\frac{\sin(2R\gamma)}{\cos(\gamma)}\cdot\left(\frac{-1}{\gamma^2}\right) \quad \text{(A-2)}$$

Since $\frac{1}{\gamma^2}$ is a second order effect, it is ignored in the following analysis. Thus, we have:

$$\frac{d}{d\gamma}\left(\frac{1}{\gamma}\cdot\frac{\sin(2R\gamma)}{\cos(\gamma)}\right)\cong\frac{1}{\gamma}\cdot\frac{d}{d\gamma}\left(\frac{\sin(2R\gamma)}{\cos(\gamma)}\right)=\frac{1}{\gamma}\cdot\frac{2R\cos(2R\gamma)\cos(\gamma)+\sin(2R\gamma)\sin(\gamma)}{\cos^2(\gamma)} \quad \text{(A-3)}$$

By studying the (A-3), it is guessed that $\gamma\to\frac{n\pi}{2}$ is the possible value that will make it zero. Let's investigate this further.

$$\lim_{\gamma\to\frac{n\pi}{2}}\frac{2R\cos(2R\gamma)\cos(\gamma)+\sin(2R\gamma)\sin(\gamma)}{\cos^2(\gamma)}=2R\cdot\lim_{\gamma\to\frac{n\pi}{2}}\left(\frac{\cos(2R\gamma)}{\cos(\gamma)}\right)+\lim_{\gamma\to\frac{n\pi}{2}}\left(\frac{\sin(2R\gamma)}{\cos(\gamma)}\right)\cdot\lim_{\gamma\to\frac{n\pi}{2}}\left(\frac{\sin(\gamma)}{\cos(\gamma)}\right) \quad \text{(A-4)}$$

By applying *L'Hopital's* rule [10], $\lim_{n\to c}\frac{f(n)}{g(n)}=\lim_{n\to c}\frac{f'(n)}{g'(n)}$ to A-4, we obtain

$$\lim_{\gamma\to\frac{n\pi}{2}}\frac{d}{d\gamma}\left(\frac{\sin(2R\gamma)}{\cos(\gamma)}\right)=2R\cdot\lim_{\gamma\to\frac{n\pi}{2}}\left(\frac{\cos'(2R\gamma)}{\cos'(\gamma)}\right)+\lim_{\gamma\to\frac{n\pi}{2}}\left(\frac{\sin'(2R\gamma)}{\cos'(\gamma)}\right)\cdot\lim_{\gamma\to\frac{n\pi}{2}}\left(\frac{\sin'(\gamma)}{\cos'(\gamma)}\right)$$

$$=2R\cdot\lim_{\gamma\to\frac{n\pi}{2}}\left(2R\cdot\frac{\sin(2R\gamma)}{\sin(\gamma)}\right)+\lim_{\gamma\to\frac{n\pi}{2}}\left(2R\cdot\frac{\cos(2R\gamma)}{\sin(\gamma)}\right)\cdot\lim_{\gamma\to\frac{n\pi}{2}}\left(\frac{\cos(\gamma)}{\sin(\gamma)}\right)=2R\cdot\left(2R\cdot\frac{\sin(\pi nR)}{\sin\left(\frac{\pi n}{2}\right)}\right)\cdot1+\left(2R\cdot\frac{\cos(\pi nR)}{\sin\left(\frac{\pi n}{2}\right)}\right)\cdot\left(\frac{\cos\left(\frac{\pi n}{2}\right)}{\sin\left(\frac{\pi n}{2}\right)}\right)$$

(A-5)

From (A-5), it is clear that when *n* takes the odd integer as $n=\pm1,\pm3,..,\gamma\to\frac{n\pi}{2}$ makes $\frac{d}{dk}(\frac{1}{\gamma}\frac{\sin(2R\gamma)}{\cos(\gamma)})=0$.

By applying *L'Hopital's* rule to A-1, we can calculate the $|c_k|$ value when $\gamma\to\frac{n\pi}{2}$.

$$|c_k|_{\gamma\to\frac{n\pi}{2}}=\left|\frac{T_1}{4RT}\cdot\frac{1}{\gamma}\cdot\lim_{\gamma\to\frac{n\pi}{2}}\frac{\sin(2R\gamma)}{\cos(\gamma)}\right|=\left|\frac{T_1}{4RT}\cdot\frac{1}{\gamma}\cdot\lim_{\gamma\to\frac{n\pi}{2}}\frac{2R\cdot\cos(2R\gamma)}{\sin(\gamma)}\right|=\frac{T_1}{T}\cdot\frac{1}{n\pi} \quad \text{(A-6)}$$

Therefore, the maximum $|c_k|$ is achieved when *n* = 1.

$$|c_k|_{max}=\frac{T_1}{T}\cdot\frac{1}{\pi}=\frac{1}{\pi}\cdot\frac{1}{1+r/I} \quad \text{(A-7)}$$

$$\gamma=\pi/2=\pi\frac{\mathrm{k}}{2\mathrm{R}}\frac{\mathrm{T}_1}{\mathrm{T}}\quad\rightarrow\quad k=\frac{T}{T_1}R=R+1/I \quad \text{(A-8)}$$

REFERENCES

[1] Liming Xiu, "The Concept of Time-Average-Frequency and Mathematical Analysis of Flying-Adder Frequency Synthesis Architecture," *IEEE Circuits and Systems Magazine*, vol. 8, No.3, pp. 27-51, Third Quarter 2008.

[2] Liming Xiu, "Some Open Issues Associated with the New Type of Component: Digital-to-Frequency Converter", *IEEE Circuits and Systems Magazine*, vol. 8, No.3, pp. 90-94, Third Quarter 2008.

[3] Liming Xiu and Zhihong You, "A Flying-Adder Architecture of Frequency and Phase Synthesis with Scalability*," IEEE Trans. VLSI Syst*., vol. 10, no. 5, pp. 637–649, Oct. 2002.

[4] Liming Xiu, "A Flying-Adder PLL Technique Enabling Novel Approaches for Video/Graphic Applications," *IEEE Transaction on Consumer Electronic*, vol. 54, pp.591-599, May, 2008.

[5] Y. C. Jenq, "Digital Spectra of Nonuniformly Sampled Signals: Fundamentals and High-speed Waveform Digitizers," *IEEE Trans. Instrum. Meas.*, vol. 37, no. 3, June 1988.

[6] Y. C. Jenq, "Digital Spectra of Nonuniformly Sampled Signals – Digital Look-up Tunable Sinusoidal Oscillator," *IEEE Trans. Instrum. Meas.*, vol. 37, no. 3, pp. 358-362, Sep. 1988.

[7] V. F. Kroupa, "Discrete Spurious Signals and Background Noise in Direct Frequency Synthesizers," *in Proc. IEEE Int. Frequency Control Symp.*, 1993, pp. 242-250.

[8] E. Curticapean and J. Niittylahti, "Exact Analysis of Spurious Signals in Direct Digital Frequency Synthesizers Due to Phase Truncations," *Electron. Lett*. vol. 39, no.6, pp. 499-501, Mar. 20, 2003.

[9] V. F. Kroupa, "Spectra of Pulse Rate Frequency Synthesizer," *Proceedings of the IEEE*, Vol. 67, No. 12, Dec. 1979.

[10] M.E. Salomon, B. Izouggaghen, A. Khouas, Y. Savaria, "Spur Model for a Fixed-Frequency Signal Subject to Periodic Jitter," *IEEE Trans. Instrum. Meas.*, vol. 57, no. 10, pp. 2320-2328, Oct. 2008.

[11] Milton Abramowitz and Irene Stegun, *Handbook of Mathematical Functions with Formulas, Graphs, and Mathematical Tables*, New York: Dover Publications, 1972.

[12] Michael H. Perrott, "Fast and Accurate Behavioral Simulation of Fractional-*N* Synthesizers and other PLL/DLL Circuits," in *DAC*, June 10-14, 2002, pp. 498-503.